Novel microstructural characteristics and properties of spray formed Al-RE-TM based alloys

V. C. Srivastava[1,2*], K. B. Surreddi[3], S. Scudino[3], M. Schowalter[4], V. Uhlenwinkel[2], A. Schulz[2], J. Eckert[3,5], A. Rosenauer[4], H.-W. Zoch[2]

[1]Metal Extraction & Forming Division, National Metallurgical Laboratory, Jamshedpur-831007, India
[2]Institut für Werkstofftechnik, Universität Bremen, Badgasteiner Str. 3, D-28359 Bremen, Germany
[3]IFW Dresden, Institute for Complex Materials, P.O. Box 27 01 16, D-01171 Dresden, Germany
[4]Institut für Festkörperphysik, Universität Bremen, Otto-Hahn-Allee 1, D-28359 Bremen, Germany
[5]TU Dresden, Institute of Materials Science, D-01062 Dresden, Germany
E-mail: vcsrivas@nmlindia.org

Abstract

Recent studies on the synthesis of bulk Al-RE (Rare Earth)-TM (Transition Metal) based alloys, from melt spun ribbons and gas atomized powders, have shown that a partially amorphous or nano-crystalline structures lead to a high specific strength. In the present study, therefore, spray atomization and deposition process has been used to produce plates of $Al_{85}Y_8Ni_5Co_2$ (deposit D1) and $Al_{83}Y_5La_5Ni_5Co_2$ (deposit D2) based alloys so as to synthesize bulk deposit of nano-crystalline and/or partial amorphous matrix composite in a single step. The rapid solidification and high undercooling of droplets during atomization and a chilling effect on undercooled liquid upon deposition are expected to give rise to the above microstructural features. The microstructural features of deposits as well as overspray powders were studied using optical, scanning and transmission electron microscope. The alloys invariably showed a large fraction of nano-crystalline and amorphous structures, characterized by featureless regions at optical resolution, along with distribution of primary equilibrium phases. The differential scanning calorimetric (DSC) analysis of the deposits showed all the crystallization peaks as is observed during crystallization of fully amorphous melt spun ribbons of respective compositions. A glass transition phenomenon is observed in Al-Y-Ni-Co based deposit. The transmission electron microscopy of deposit D1 showed the presence of 50-100 nm size fcc-Al precipitates in an amorphous matrix decorated with 5-20 nm fcc-Al crystallites. The annealing treatment of deposits at different temperatures, determined from the crystallization peaks of the deposit, showed precipitation of nanoscale fcc-Al and intermetallic phases giving rise to a remarkable increase in hardness. The bulk hardness of the deposits D1 and D2 was 391 and 427 HV, respectively. Whereas, the heat treated deposits showed a bulk hardness value of 476 HV for deposit D1 at 298 ^oC and 582 HV for deposit D2 at 380 ^oC. An attempt has been made to bring out the possible mechanism of microstructural evolution during spray deposition of these alloys, and the effect of microstructural features on the mechanical properties has been discussed.

1. Introduction

In the recent years, several attempts have been made to synthesize bulk nano-crystalline or nano-crystalline/amorphous Al-Rare Earth-Transition Metal based alloys so as to achieve high specific strength with appreciable ductility. The high strength of these alloys is generally attributed to the formation of high number density of nanoscale fcc-Al phase in an amorphous matrix [Ino98, Gög02, Cho95, Kaw01, Wan06]. In other attempts, a high strength (≈1000-1200 MPa) has also been observed after hot consolidation of amorphous precursors which leads to bulk nano-crystalline structure [Kaw01, Wan06, Wan08, Glo03, Ino88, Sen05]. Mostly, the synthesis of bulk materials is accomplished by using melt spun amorphous ribbons [Ino88] or gas atomized amorphous powders (<20 μm) as the precursor material [Sen05]. A few recent attempts have been made to synthesize variants of these alloys by spray forming process [Afo03, Gol03, Afo01, Guo06, Guo05]. These studies report the formation of only a small fraction of amorphous phase in the deposit up to only 1-2 mm thickness from the substrate surface. These are particularly achieved, as reported, either by using cryogenic temperature on substrates [Sen05, Afo03] to allow efficient heat extraction or by using a high gas to metal (G/M) ratio of 10 m^3/kg [Gol03, Afo01] for droplet refinement and thus high cooling rate. However, a high G/M ratio leads to large fraction of cold/interstitial porosity (around 10-15%) and in the case of using a cold substrate, the thermal stresses and shrinkage of the liquid during initial splat/layer on the substrate leads to the detachment of the deposit from the substrate, which results in heat accumulation in the deposit and ineffective heat removal during further deposition [Guo06]. Therefore, it becomes necessary to obviate the above limitations by modifying the process parameters to achieve better heat removal during deposition and study the mechanism of microstructural evolution, which is not yet clearly understood, for such alloys.

Therefore, in the present investigation, attempt has been made to synthesise 10-12 mm thick plates of Al-Y-Ni-Co and Al-Y-La-Ni-Co alloys by spray forming and characterise their microstructure and mechanical properties. The results have been discussed in light of the droplet solidification prior to deposition and the mechanism of their interaction with the substrate.

2. Experimental details

In the present investigation, a 10-12 mm thick, 250 mm wide and 600 mm long plates of $Al_{85}Y_8Ni_5Co_2$ (deposit D1) and $Al_{83}Y_5La_5Ni_5Co_2$ (deposit D2) by spray forming, using a 30 mm thick copper substrate pre-heated to 110 ^oC and 160 ^oC, respectively. The thick substrate was chosen to utilize the high heat capacity of the substrate and the pre-heating was done to affect a close contact at the deposit/substrate interface to enhance the heat removal. The pure materials (for Ni: Al-20Ni master alloy) were induction melted in a purified argon atmosphere and atomized with nitrogen gas. A large deposition distance of 700 mm was used. The G/M ratio of 5.39 and 7.72 kg/kg was used for deposit-D1 and deposit-D2, respectively. The melt flow rates were 239 kg/h and 154 kg/h for the deposit-D1 and deposit-D2 respectively. The spray was scanned on the substrate at a frequency of 15.2 Hz within a scan angle of $\pm 10.5^o$. The spray deposited material was immediately cooled using nitrogen gas at a pressure of 0.2 MPa. The spray deposited material was examined under optical and scanning electron microscope (SEM). The differential scanning calorimetric (DSC) analysis was carried out using a Perkin-Elmer diamond calorimeter at a heating rate of 40 ^oC/min under a continuous flow of purified argon. The x-ray diffraction (XRD) analysis was done using Co-K radiation for the as-deposited materials both before and after DSC analysis up to 500 ^oC. The deposit-D1 was also studied by transmission electron microscopy (TEM) using a TITAN

80/300 microscope equipped with scanning TEM with a resolution of 0.136 nm. The TEM samples were prepared by grinding to a thickness of about 70 μm followed by ion beam etching, using a Gatan "precision ion polishing system" (PIPS), with Xe ions from both sides with an angle of ± 5° and an acceleration voltage of 5 KeV.

The as-spray deposited materials were further processed by melt spinning to produce amorphous ribbons so as to compare the deposits with that of the completely amorphous material characteristics. The ribbons were produced using a copper wheel at a tangential velocity of 44 m/s. The spray deposited materials were annealed at different temperature, based on the exothermic peaks in the DSC scans, to assess the microstructural modification of the deposits. The Vickers hardness was measured at a load of 0.25 N for individual phases and at 2.0 N for bulk material.

3. Results

3.1 Optical microscopy

The composition of the alloys taken in this study is far from the eutectic composition and therefore a coarse primary phase is expected in a eutectic matrix during equilibrium cooling. However, in melt atomization, the high cooling rate of droplets lead to refinement of primary phases. Fig. 1 (a and b) shows the optical micrographs of $Al_{85}Y_8Ni_5Co_2$ and $Al_{83}Y_5La_5Ni_5Co_2$ powders, in the size range of 50-75 μm, depicting featureless as well as

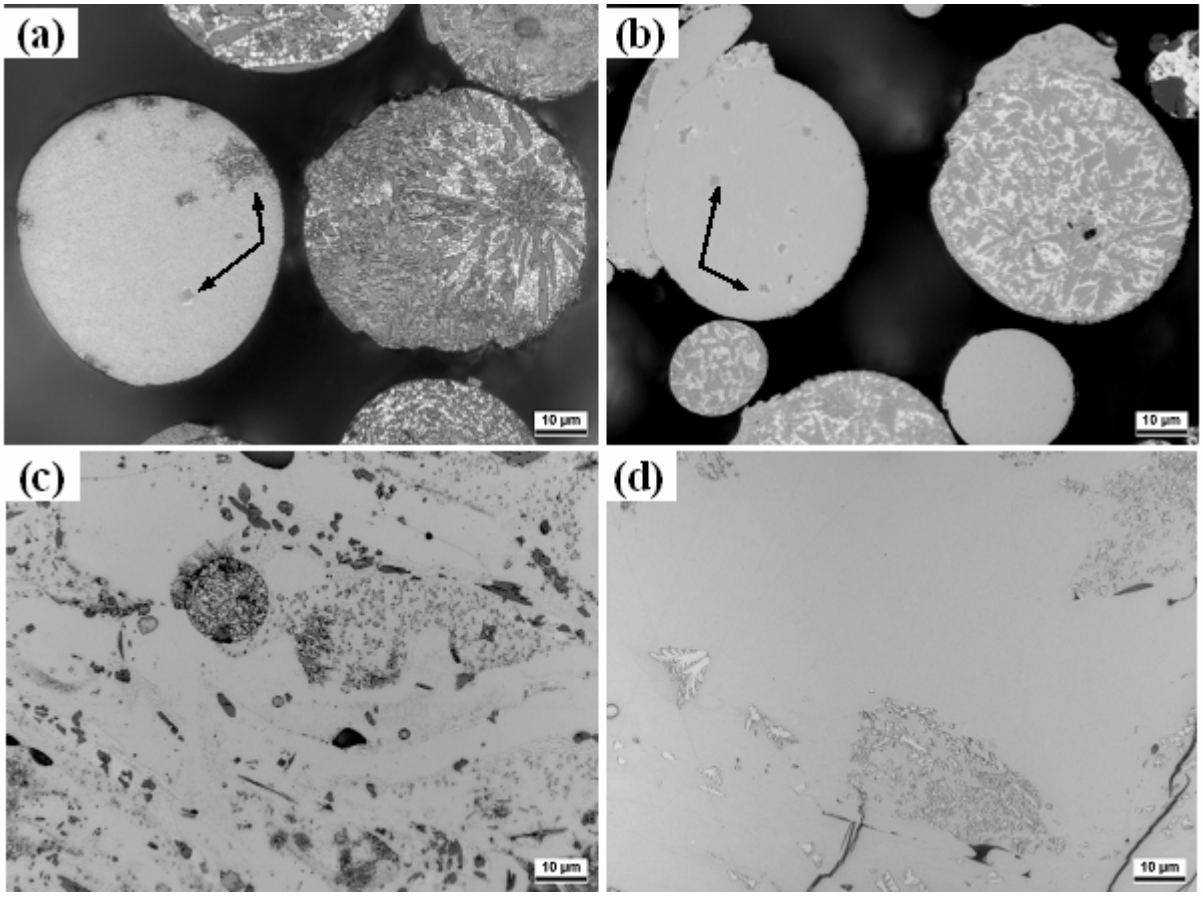

Figure 1: Optical micrographs of (a and b) $Al_{83}Y_5La_5Ni_5Co_2$ and $Al_{85}Y_8Ni_5Co_2$ powders in coarse-structured particles. the size range of 50-75 μm and (c and d) deposit-D2 and deposit-D1, respectively.

coarse-structured particles. The droplets witnessing high undercooling give rise to featureless structure, whereas those slowly cooled or having heterogeneous nucleation sites lead to coarse structure with large size primary phases. A large number of particles were observed to have a primary phase in an almost featureless matrix. The primary phases in such particles is marked by arrows in fig. 1 (a and b). Fig. 1 (c and d) shows the optical micrographs of the deposits, deposit-D1 and deposit-D2 respectively, which depicts large fraction of featureless areas in the deposits, with some metastable or primary intermetallic phases, compared to the coarse structure of large size powder particles depicted in fig. 1a and 1b. The deposits also revealed a few pre-solidified featureless particles as well as particles with coarse structure. Both the deposits showed different primary phase morphologies which are expected to arise due to various solidification conditions witnessed by the atomized droplets prior to deposition.

3.2 Differential scanning calorimetry and X-ray diffraction

Fig. 2a shows the DSC heat flow curves for spray deposits and the melt-spun ribbons of the same compositions i.e. $Al_{83}Y_5La_5Ni_5Co_2$ and $Al_{85}Y_8Ni_5Co_2$. The $Al_{85}Y_8Ni_5Co_2$ alloy shows exothermic three peaks similar to fully amorphous melt spun ribbons. Similarly, $Al_{83}Y_5La_5Ni_5Co_2$ alloy shows two peaks. However, the crystallization energy for the first peak, in both the deposits, is less compared to the melt-spun ribbons. This indicates the partially amorphous condition of the deposits. When compared with the first peak crystallization energy of melt-spun ribbons, $Al_{83}Y_5La_5Ni_5Co_2$ and $Al_{85}Y_8Ni_5Co_2$ alloys indicated an amorphous fraction of about 37%. Whereas, comparing from the total crystallization energy, the alloy showed an amorphous fraction of 47.6 and 74.6%, respectively. However, a glass transition phenomenon was observed only in the $Al_{85}Y_8Ni_5Co_2$, which was around 275 ^oC.

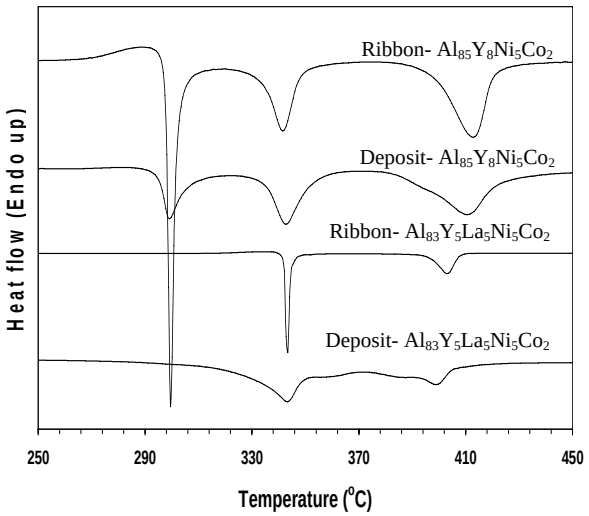

Fig. 2a: DSC scan curves for ribbons and deposits of $Al_{83}Y_5La_5Ni_5Co_2$ and $Al_{85}Y_8Ni_5Co_2$

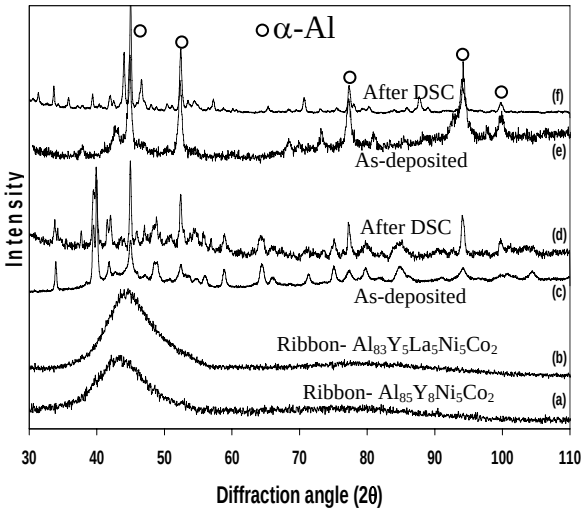

Fig. 2b: XRD diffraction patterns for (a and b) Ribbon (c and d) $Al_{83}Y_5La_5Ni_5Co_2$ and (e and f) $Al_{85}Y_8Ni_5Co_2$

Fig. 2b shows the x-ray diffraction patterns of the melt spun ribbons, the as-deposited materials and the deposits after DSC scan up to 500 ^oC. The melt spun ribbons clearly shows the amorphous nature. The as-sprayed deposit of $Al_{85}Y_8Ni_5Co_2$ alloy mainly showed the presence of a-Al and supersaturated Al_2Y and some unknown phases, whereas, $Al_{83}Y_5La_5Ni_5Co_2$ showed the existence of a-Al, $Al_{11}La_3$, Al_3Y and some unknown phases. However, after DSC, $Al_{85}Y_8Ni_5Co_2$ alloy indicated precipitation of Al_3Y and Al_9Co_2. In spray

deposited material, peak broadening was clearly observed in comparison with the peaks obtained after DSC scan.

3.3 Scanning and transmission electron microscopy

The scanning electron microscopy showed different scales of microstructure in the featureless areas as well as the areas between the primary phases. Fig. 3 (a and b) shows the microstructure in the featureless regions and between the fragmented dendrites of the primary phase in $Al_{83}Y_5La_5Ni_5Co_2$ alloy. It is obvious that the scale of microstructure varies between 100-200 nm. The difference in microstructure scale depends upon the solidification condition and the undercooling of droplets upon deposition. The areas between the dendrite fragments also reveal nanostructure. Similarly, $Al_{85}Y_8Ni_5Co_2$ alloy showed highly refined nanoscale structure in the featureless areas (fig. 3c). It seems that eutectic-like colonies grow at the surface of fine secondary phases. In $Al_{85}Y_8Ni_5Co_2$ alloy, a considerable area fraction revealed the presence of fine secondary nucleated particles of 200-600 nm. A highly refined structure seems to grow around these particles (fig. 3d). The scale of microstructure varied even in the featureless areas, which is due to the cooling condition of droplets before deposition. However, featureless regions invariably indicated nanoscale structure. A considerable area fraction was not resolvable by SEM and, therefore, transmission electron microscopy was carried out to resolve such areas.

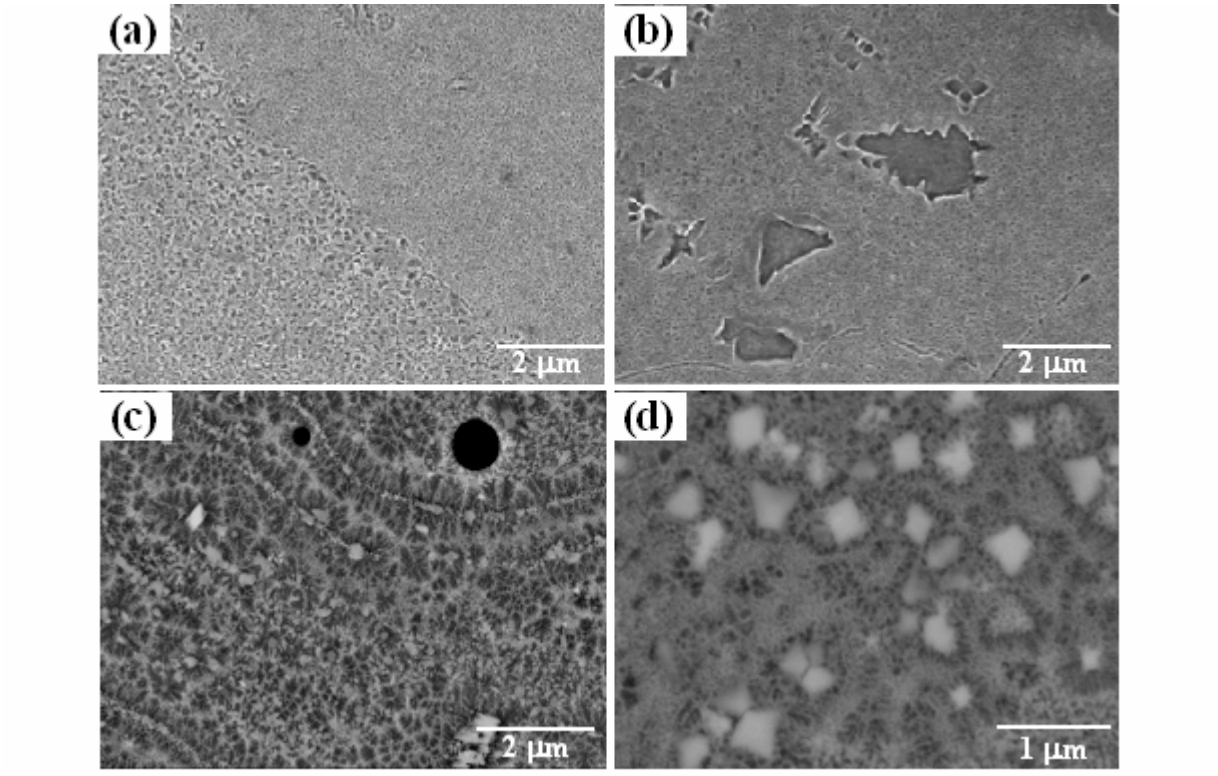

Fig. 3: Scanning electron micrographs of as-sprayed deposits of (a and b) $Al_{83}Y_5La_5Ni_5Co_2$ (c and d) $Al_{85}Y_8Ni_5Co_2$ alloy depicting ultrafine microstructural features.

The thermal analysis, XRD and scanning electron microscopy did not reveal the full information about the materials so far as the morphological characteristics of the various phases are concerned. Therefore, transmission electron microscopy was carried out to resolve the nanostructured features in the deposit. The TEM analysis of $Al_{85}Y_8Ni_5Co_2$ alloy mainly

indicated the presence of Al_2Y and Al_3Y particles in the size range of 200-600 nm surrounded by a nano-crystalline matrix. The interface regions of the intermetallic particles indicated the rejection of Al in the matrix and the area around the particles were decorated with nanoscale α-Al grain with amorphous boundaries. The larger size primary phase, as shown in fig. 1 (c and d) could not be seen in thin sample areas under TEM. The matrix consists of a partially crystallized amorphous phase (in gray contrast in fig. 4a) and 100-150 nm Al grain (white contrast in fig. 4a). The selected area diffraction (SAD) pattern shows a diffuse ring with spots from crystals. A higher magnification micrograph (fig. 4b) shows the amorphous phase in gray contrast and α-Al in white. The white fine particle (5-20 nm) within the amorphous phase is the Al precipitates formed during crystallization of amorphous matrix. The SAD patterns of crystalline and amorphous regions are shown. In contrast, $Al_{83}Y_5La_5Ni_5Co_2$ system showed fully amorphous regions separated by nanocrystalline regions (fig. 4c). The SAD pattern of the amorphous regions showed a fully diffused ring without any diffraction spots from crystals. The nanocrystalline regions showed splitting of diffraction spots and a discrete ring pattern. In some areas, very fine structure were observed revealing the development of α-Al dendrites in an amorphous matrix (fig. 4d). The presence of Al was confirmed by EELS measurement. The gray areas in fig. 4d showed a diffraction pattern with diffuse ring, whereas, the dendritic region showed crystalline spots, as shown in insets in fig. 4d.

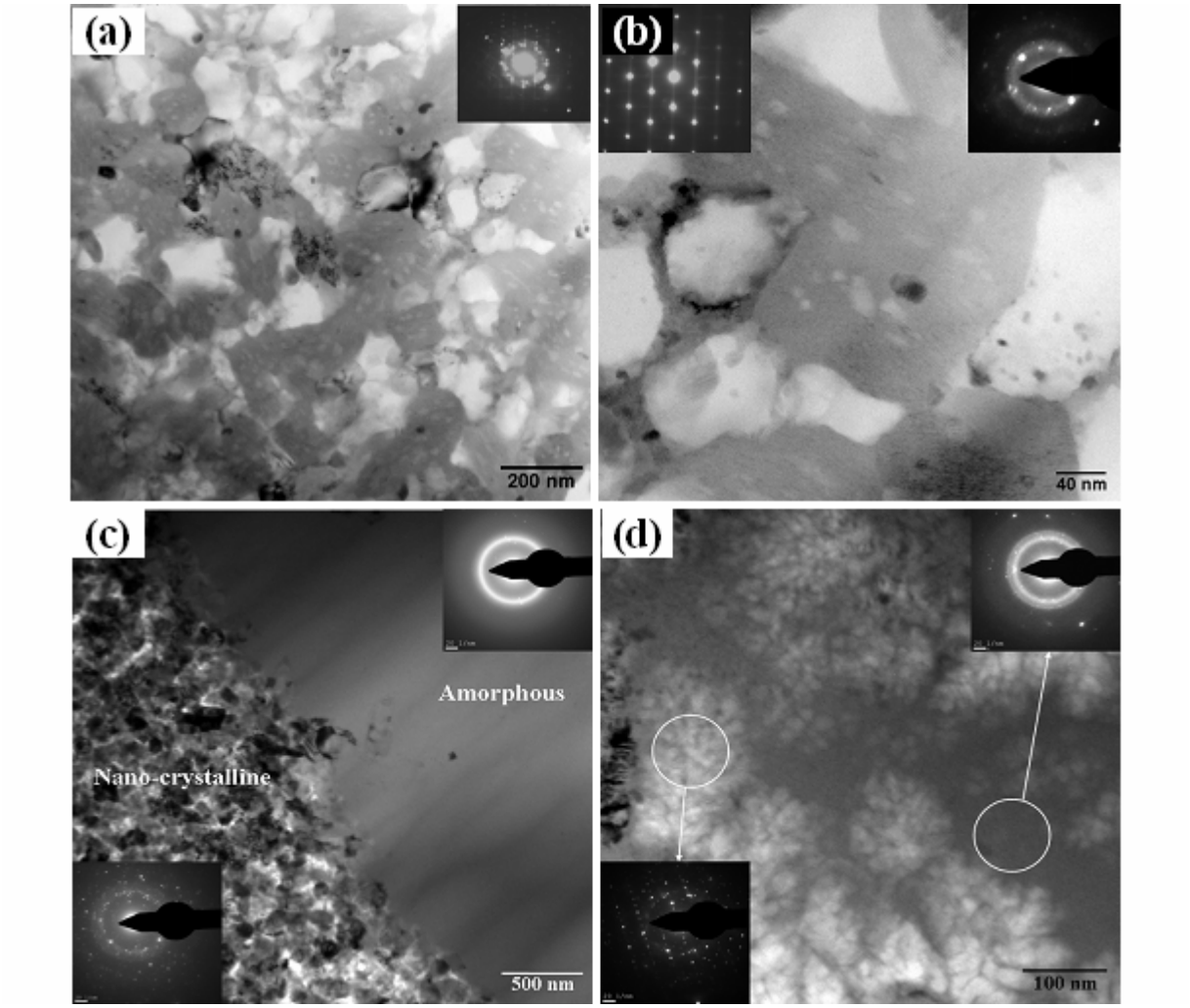

Fig. 4: TEM micrographs showing (a) a-Al grain in amorphous matrix (b) small Al rich phase formation in $Al_{85}Y_8Ni_5Co_2$ alloy and (b) coexisting amorphous and nanocrystalline regions and (d) Al dendrites in an amorphous matrix in $Al_{83}Y_5La_5Ni_5Co_2$ alloy.

3.4 Mechanical properties

As the deposits showed a large fraction of amorphous phase in the microstructure, mechanical property characterization was undertaken to evaluate the hardness and compressive strength of the deposits. Hardness was measured after annealing the samples at different transformation reaction temperature indicated by DSC flow curves. Fig. 5 (a and b) shows the plots depicting hardness values in as-deposited and annealed condition for bulk and featureless regions.

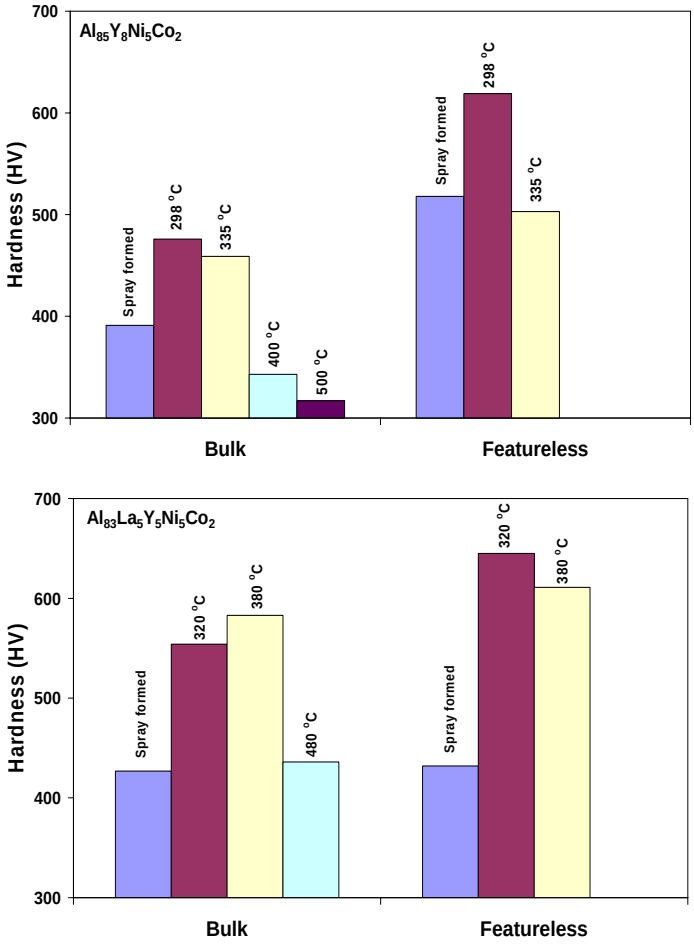

Fig. 5: Hardness values of bulk and featureless regions in (a) $Al_{85}Y_8Ni_5Co_2$ and (b) $Al_{83}Y_5La_5Ni_5Co_2$ deposits before and after annealing at different temperatures for 15 min.

The bulk hardness value for as-deposited $Al_{85}Y_8Ni_5Co_2$ alloy is 391 HV which reaches to a maximum of 476 HV after annealing at 298 ^oC for 15 min. Whereas, the featureless regions showed a maximum hardness of 640 HV in the same anneal condition. In contrast, a high bulk hardness of 583 HV is observed for $Al_{83}Y_5La_5Ni_5Co_2$ alloy deposit after annealing at 380 ^oC, in contrast to 427 HV in as-deposited condition. The hardness of featureless regions is 670 HV after annealing at 320 ^oC. These hardness values are close to the maximum hardness values reported for the alloys based on Al-RE-TM system. The spray deposit and overspray powders (50-75 μm size range) of $Al_{85}Y_8Ni_5Co_2$ alloy were extruded at 450 ^oC and their compressive strength were evaluated. The compression test behaviour of the as-spray deposited as well as the extruded materials is shown in fig. 6. The as-deposited alloy showed high strength of around 800 MPa despite a porosity volume fraction of 7%. The extruded powder, which contained around 32% amorphous fraction based on total crystallization

energy, revealed a strain hardening effect but showed a low fracture strain of 3%. In contrast, the spray formed and extruded material showed the strength of 925 MPa along with a high fracture strain of 9%.

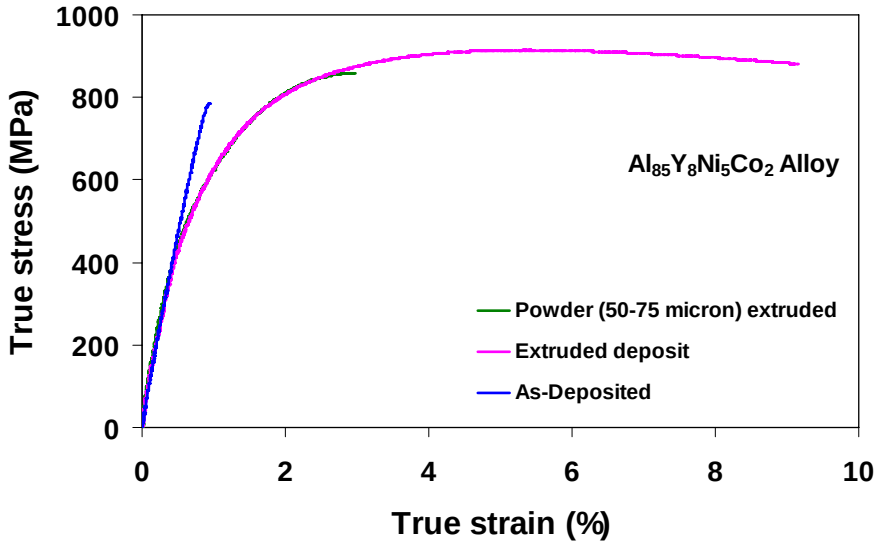

Fig. 6: Compression test flow curves for $Al_{85}Y_8Ni_5Co_2$ alloy in different processing conditions

4. Discussion

Spray forming process combines two separate processes of melt atomization into spray of a wide size range of micron-size droplets and its deposition onto a substrate. The disintegration of melt with high velocity inert gas jets leads to formation of small droplets which experience a high cooling rate due to convective and radiative mode of heat transfer during flight in the spray. The cooling rate of droplets varies in the range of 10^3-10^6 K/s depending upon their size or specific surface area, which determines their solidification conditions during flight in the spray and prior to deposition on the substrate. The degree of undercooling of the droplets prior to the commencement of solidification increases with increasing cooling rate [Lav96, Gra95, Das01]. However, a droplet may experience small undecooling in the presence of a potent heterogeneous nucleation site in the droplet. These conditions, therefore, lead to a highly inhomogeneous solidification structure in as-solidified overspray particles, as shown in fig. 1 (a and b). A large particle, which might have no potent heterogeneous nuclei and would have experienced a high undercooling, reveals highly metastable and featureless structure. The droplets with smaller degree of undercooling solidify with the formation of coarse primary phases and eutectic matrix. Whereas, most of the small droplets, which witness high cooling rate, gives rise to large fraction of featureless regions. The investigated alloys in the present study possess high glass forming ability among the glass forming aluminium alloys. Therefore, the undercooled liquid in the droplets possesses high viscosity below the liquid temperature resulting in sluggish kinetics of atomic diffusion. Therefore, even if there is a partial crystallization in the droplets, the remaining continuously-cooled liquid may have sluggish diffusion leading to nano-crystallization or amorphization [Kal08].

Due to varying cooling rate of droplets, smaller droplets are solidified well before deposition, whereas, larger droplets remain in undercooled state. The intermediate size droplets deposit on the substrate either in the highly undercooled state or partially solidified condition, the remaining liquid being highly viscous. The deposition of the semi-solid or liquid droplets onto the substrate or the growing deposit leads them to make a thin splat on the

surface which experiences a high cooling rate due to low deposit temperature, as has been discussed later. As a pre-heated and thick substrate was used in the experiments, large amount of heat is rapidly extracted from the deposit into the substrate through conduction due to a close contact between the substrate and the deposit. Therefore, the heat accumulation, with the increase in deposit thickness, is avoided. The temperature of the deposit and the substrate was measured during and after the deposition process and is shown in fig. 7. The details of the positions of the thermocouples in the substrate and the deposit can be found in Ref. [Sri09]. The temperature curves, shown in the figure, are for the thermocouples which come in the contact with the spray cone first (Thermocouples TD1 and TS1 in fig. 1 in ref. [Sri09]). The temperature curves show that the maximum temperature in the $Al_{83}Y_5La_5Ni_5Co_2$ deposit (D2) is close to 250 ^oC and in the in the $Al_{85}Y_8Ni_5Co_2$ deposit (D1) it is around 290 ^oC. The maximum temperatures are less than the temperature for the first transformation, as found from DSC analysis, for both the alloy. However, as the temperatures were measured only at 3 mm from the substrate surface it may be possible that the temperature in the deposit may rise to a higher value due to its large thickness. But it is expected that this temperature rise will not be highly significant, which has also been manifested by the presence of amorphous phase in the middle of the deposit thickness. The low deposit temperature indicates efficient heat extraction from the droplet splats.

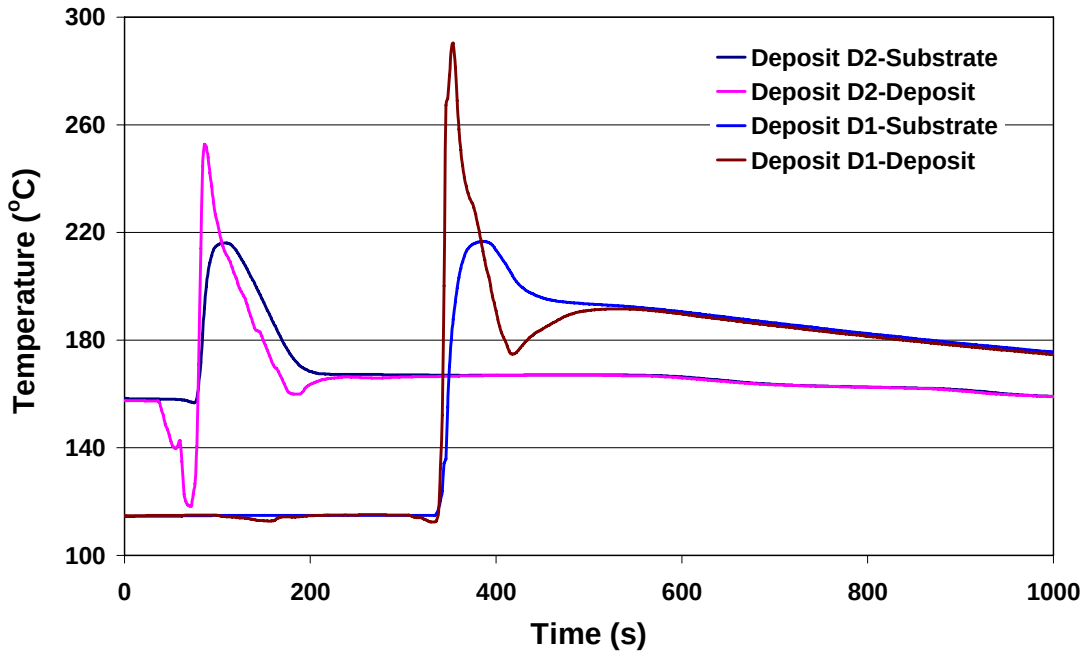

Fig. 7: Temperature variation in the deposit and the substrate; before, during and after the completion of the deposition process. The time scale is absolute for both the experiments.

The deposit microstructure was observed to be locally inhomogeneous due to the deposition of droplets having various degrees of undercooling which determines the final solidification structures upon deposition. This is manifested from the microstructural features of the deposit where the nanocrystalline region is coexisting with the amorphous phase (fig. 4c) and the α-Al dendrites are formed in an amorphous matrix (fig. 4d). In the complex alloys, as in the present case, the sequence of equilibrium solidification is modified in a highly non-equilibrium case of undercooled droplets. Therefore, in some cases highly undercooled large droplets may solidify with α-Al as the primary phase. Whereas, droplets with relatively low undercooling may lead to the formation of equilibrium primary phases followed by solidification of remaining liquid during chilling on the deposition surface. The

inhomogeneity in the heat content of the droplets prior to deposition may also present different temperatures for the incoming depositing droplets. This may lead to the variation in the cooling rate during splating and chilling. This condition becomes valid here because of the fact that the incoming liquid arrive in highly viscous condition and therefore the possibility of long range temperature equilibration becomes low. This is in contrast to spray forming of conventional alloys where a liquid pool is formed which gives rise to a uniform local surface condition. However, the absence frequent prior particle boundaries does indicate that the temperature of the incoming liquid and its fluidity remains enough for a proper bonding between the deposit and the incoming droplets. It can be concluded from the above discussion that the deposit consists of a microstructure which is locally inhomoheneous but consists of a large fraction of amorphous and nanocrystalline features along with a distribution of primary intermetallic phases.

The presence of nanocrystalline and amorphous phases in the deposits gave an opportunity for tailoring the microstructure with respect to the crystallization and grain growth in these phases, which were featureless at the optical resolution. Therefore, the deposits were annealed for 900 seconds at different temperatures corresponding to the crystallization peaks obtained from the DSC measurements. The $Al_{85}Y_8Ni_5Co_2$ alloy showed an increase in the hardness after annealing at 298 ^oC, where nanoscale Al precipitates form in the amorphous matrix. But the second transformation, beginning at around 335 ^oC, leads to the formation of long rods of intermetallic phases which may be attributed to lower hardness. The bulk hardness, which can be said to be the average hardness of the deposit, also shows highest value at 298 ^oC indicating that hardness value is mainly derived from the crystallized amorphous areas. A very low hardness values, after annealing above 400 ^oC, is attributed to the full transformation of the amorphous phases into coarse intermetallic phases. In contrast to the formation of long rods of intermetallic phases, it was observed in TEM experiments with in-situ heating arrangement that the amorphous areas in $Al_{83}Y_5La_5Ni_5Co_2$ alloy gave rise to cluster like solute rich areas in an amorphous matrix at the first transformation temperature beginning at around 320 ^oC. At the annealing temperature of 380 ^oC a rapid transformation of amorphous matrix into nanoscale structure was observed. However, further increase in the temperature upto 500 ^oC only led to coarsening of the nanoscale features. The already existing coarse nanoscale features (fig. 4c) did not grow significantly even at the high temperature of above 500 ^oC. This indicated that the $Al_{83}Y_5La_5Ni_5Co_2$ alloy was highly stable at high temperatures and maintained a nanoscale structure. However, it is difficult to suggest anything with respect to the long annealing time as the TEM heating was limited to 600 s. The high hardness of the $Al_{83}Y_5La_5Ni_5Co_2$ alloy at 380 ^oC may be attributed, therefore, to the nanoscale (10-40 nm) intemetallic features formed from the amorphous matrix.

These results presented here are the initial reports of the study and further analysis of the results are in progress. However, this study effectively indicated the efficacy of the spray forming process to develop materials with a combination of microstructural features along with appreciable mechanical properties. There exists a possibility to modify the process parameters as well as the atomization techniques to obtain smaller droplet size with narrow size distribution so as to achieve large fraction of highly undercooled droplets with similar solidification behaviour. This can give better microstructural homogeneity in the deposit.

Acknowledgments

The authors would like to thankfully acknowledge the financial support from the German Research Foundation (DFG) under SFB-Transfer Program 58 of the University of Bremen, Germany. Dr. Srivastava would like to thank Alexander von Humboldt Foundation (Germany) for granting the fellowship for supporting his stay in Germany and the Council of

Scientific and Industrial Research (India) for granting him the leave to pursue this research work.

References

[Afo01] C.R.M. Afonso, C. Bolfarini, C.S. Kiminami, N.D. Bassim, M.J. Kaufman, M.F. Amateau, T.J. Eden, J.M. Galbraith: *Amorphous phase formation in spray deposited AlYNiCo and AlYNiCoZr alloys*, Scripta mater. 44 (2001), 1625–1628

[Afo03] C.R.M Afonso, C. Bolfarini, C.S. Kiminami, N. D. Bassim, M.J. Kaufmann, M.F. Amateau, T.J. Eden, J. M. Galbraith: *Amorphous phase formation during spray forming of $Al_{84}Y_3Ni_8Co_4Zr_1$ alloy*, J. Non-Cryst. Solids 284 (2003), 134-138

[Cho95] G.S. Choi, Y.H. Kim, H.K. Cho, A. Inoue, T. Masumoto: *Ultrahigh tensile strength of amorphous Al-Ni-(Nd,Gd)-Fe alloys containing nanocrystalline Al particles*, Scripta Mater. 33 (1995), 1301-1306

[Das01] S.K. Das, J.H. Perepezko, R.I. Wu RI, G. Wilde: *Undercooling and glass formation in Al-based alloys*, Mater. Sci. Eng. A 304-306 (2001), 159-165

[Glo03] T. Gloriant : *Microhardness and abrasive wear resistance of metallic glasses and nanostructured composite materials*, J. Non-Cryst. Solids 316 (2003), 96-103

[Gog02] M. Gögebakan: *Mechanical properties of AlYNi amorphous alloys*, J. Light Met. 2 (2002), 271-275

[Gol03] W.J. Golumbfskie, M.F. Amateau, T.J. Eden, J.G. Wang, Z.K. Liu: *Structure–property relationship of a spray formed Al–Y–Ni–Co alloy*, Acta Materialia 51 (2003), 5199–5209

[Gra95] P.S. Grant: *Spray forming*, Prog. Mater. Sci. 39 (1995), 497-545

[Guo05] M.L.T. Guo, C.Y.A. Tsao, J.C. Huang, J.S.C. Jang: *Crystallization behavior of spray-formed and melt-spun $Al_{89}La_6Ni_5$ hybrid composites with amorphous and nanostructured phases*, Mater. Sci. Eng. A 404 (2005), 49-56.

[Guo06] M.L. T Guo, Chi Y.A. Tsao, J.C. Huang, J.S.C. Jang: *Microstructural evolution in spray-formed and melt-spun $Al_{85}Nd_5Ni_{10}$ bulk hybrid composites*, Intermetallics 14 (2006), 10691074

[Ino88] A. Inoue, K. Othera, A.P.Tsai, T. Mosumoto: *Aluminium based amorphous alloys with tensile strength above 980 MPa*, Japan. J. Applied Phys. 27 (1988), L479-L482

[Ino98] A. Inoue: *Amorphous, nanoquasicrystalline and nanocrystalline alloys in Al-based systems*, Prog. Mater. Sci. 43 (1998), 365-520

[Kal08] Y.E. Kalay, L.S. Chumbley, I.E. Anderson: *Characterization of a marginal glass former alloy solidified in gas atomized powders*, Mater. Sci. Eng. A 490 (2008), 72-80.

[Kaw01] Y. Kawamura, H. Mano, A. Inoue: *Nanocrystalline aluminum bulk alloys with a high strength of 1420 MPa produced by the consolidation of amorphous powders*, Scripta mater. 44 (2001), 1599-1604

[Lav96] E. J. Lavernia, Y. Wu, Spray Atomization and Deposition, John Wiley and Sons, West Sussex, England, 1996, pp. 155-260.

[Sen05] O.N. Senkov, S.V. Senkova, J.M. Scott, D.B. Miracle: *Compaction of amorphous aluminum alloy powder by direct extrusion and equal channel angular extrusion*, Mater. Sci. Eng. A 393A (2005) 12-21.

[Sri09] V.C. Srivastava, K.B. Surreddi, V. Uhlenwinkel, A. Schulz, J. Eckert, H.-W. Zoch: *Formation of Nanocrystalline Matrix Composite during SprayForming of Al83La5Y5Ni5Co2*, Metall. Mater. Trans. A 40 (2009), 450-461

[Wan06] Y.B. Wang, H.W. Yang, B.B. Sun, B. Wu, J.Q. Wang, M.L. Suia, E. Ma: *Evidence of phase separation correlated with nanocrystallization in $Al_{85}Ni_5Y_6Fe_2Co_2$ metallic glass*, Scripta Mater. 55 (2006), 469-472

[Wan08] Y. Wang, R.S. Mishra, T.J. Watson: *Mechanical behavior of devitrified ultrafine-grained Al–4.0Y–4.0Ni–0.9Co matrix composites*, Scripta Mater. 59 (2008), 1079-1082